Sentinels4Carbon (Sense4Fire)

Sentinel-based fuel, fire and emissions products to constrain the changing role of vegetation fires in the global carbon cycle

ESA Contract Number: 4000134840/21/I-NB

Product Validation Report Version 1.1

(PVRv1)

11 November 2022, Version 1.1

Prepared by:

Matthias Forkel, Christine Wessollek, Daniel Kinalczyk, Christopher Marrs

Technische Universität Dresden, Faculty of Environmental Sciences, Dresden, Germany

Vincent Huijnen, Jos de Laat, Martin de Graaf

Royal Netherlands Meteorological Institute (KNMI), De Bilt, The Netherlands

Niels Andela, Alfred Awotwi

Cardiff University, School of Earth and Environmental Sciences, Cardiff, Wales, UK

Contents

Figures

Tables

Acronyms

AAI	Absorbing Aerosol Index
AGB	Above Ground Biomass
AIC	Akaike's Information Criterion
ALH	Aerosol Layer Height
ATBD	Algorithm Theoretical Baseline Document
BAAD	Biomass and Allometry Database
CAMS	Copernicus Atmosphere Monitoring Service
CCI	Climate Change Initiative
DRC	Democratic Republic of Congo
ESA	European Space Agency
GAM	Generalised Additive Model
GEDI	Global Ecosystem Dynamics Investigation
GFAS	Global Fire Assimilation System
GFED	Global Fire Emission Database
IFS	Integrated Forecasting System
LAI	Leaf Area Index
LFMC	Live Fuel Moisture Content
MOPITT	Measurement of Pollution in the Troposphere
OMI	Ozone Monitoring Instrument
PVP	Product Validation Plan
PVR	Product Validation Report
SLA	Specific Leaf Area
SMAP	Soil Moisture Active Passive
TROPOMI	TROPOspheric Monitoring Instrument
VIIRS	Visible Infrared Imaging Radiometer Suite
VOD	Vegetation Optical Depth
VODCA	Vegetation Optical Depth Climate Archive
WP	Work Package

1 Introduction

This Product Validation Report version 1 (PVRv1) describes the strategy, plans and first results for product calibration and validation for methods and products that are developed within the ESA-funded Sense4Fire project: Sentinel-based fuel, fire and emissions products to constrain the changing role of vegetation fires in the global carbon cycle. The aim of Sense4Fire is to increase the scientific understanding of fire dynamics and their role in the carbon cycle by integrating observations from the Sentinels into new Earth observation products.

The validation of data products is crucial for the evaluation of the complex production chain underlying the Sense4Fire project: Algorithms that combined data from either Sentinel 1-2-3 into data products, algorithms that merge those data products into emissions, CAMS/IFS model simulations that use those emissions to simulate the spatio-temporal structure of the chemical composition of the atmosphere, and Sentinel-5p atmospheric composition data that is used to validate and re-calibrate those model simulation results. Differences between the CAMS/IFS model simulation and Sentinel-5p observations thus can be caused by one of the many processes in the Sense4Fire production chain. Hence the validation should not only focus on the comparison between model results and Sentinel-5p data, but also on the validation of individual data products further down the production chain. Understanding and quantifying errors and uncertainties is important to identify where and when the production chain can be improved. The validation may lead to immediate data product improvement, but equally to identification of data product limitations that cannot be immediately resolved and require additional action. The latter will find its way into a gap analysis that will be part of the PVR and final project report. The gap analysis can be used to initiate or support additional research and development activities beyond the Sense4Fire project end.

PVRv1 builds on the description of methods and algorithms from the Algorithm Theoretical Baseline Document version 1 (ATBDv1). ATBDv1 focuses on method development using specific case study areas and hence PVRv1 describes first calibration/validation results for selected case study areas. An overview of the study areas is provided Chapter 2 in the ATBDv1- The actual validation of the methods, algorithms and data products will take place during the second half of WP3 and corresponding results will be presented in Version 2 of the ATBD and PVR (ATBDv2 and PVRv2), which are due by the end of November 2022. ATBDv2 and PVRv2 will also describe the application of the methods and derived products to larger areas.

Chapter 2 presents validation results for the classification of fire types. Chapter 3 presents calibration, test and benchmarking results of the fuel model with respect to tree height and biomass compartments. In Chapter 4, we then describe the validation plan for methods to estimate fire emissions from a top-down approach using Sentinel-5p observations.

2 Burned area and fire behaviour

This project component aims to deliver three products. First, we track individual fire perimeters as objects at a daily temporal resolution. Second, we classify these objects as specific fire types, for example forest, deforestation, or savannah fires. Third, we estimate and scale burned area for each object, a critical step for estimating fire emissions. Each step requires training and quality assessment, training efforts are clarified in the ATBDv1 and details about quality assessment are provided here.

2.1 Tracking fire objects

Our aim is to identify individual wildfires and track the daily expansion of the fire perimeter. Defining a 'wildfire' itself can be difficult at times, as each continuous burned area can include multiple ignition locations sometimes driven by the fire itself (e.g., spotting). The precise definition of fire objects, and subsequent estimates of fire perimeters, has an indirect influence on our emissions estimates as it determines the aggregate fire properties and therefore the fire type and attributed burned area of each object. Here we use the Global Fire Atlas algorithm (Andela et al., 2019) to track individual wildfires at each time step. In open cover types with rapid fire spread rates, active fire detections do not provide full coverage of the fire extent and fire events become fragmented in our approach. We do not account for this in our fire tracking algorithm, since the fire types for open cover are directly dependent on land cover type, but not fire behaviour or other fire attributes. Instead, we scale burned area for each object to provide robust estimates of burned area across larger scales. Given the large and long-term impacts of fires in forested systems on carbon emissions, our focus is on woodland and forest fires, which are generally well captured by active fire detections. Here we use our Sentinel-2 based burned area estimates (continuous burned area) in combination with visual interpretation of the burn date from the active fire detections to derive a small (50-100 fires) set of reference fires for each study region (Brazil, Russia, southern Africa) to provide additional quality assessment of fire perimeters in closed cover types in addition to the assessment provided by Andela et al., 2019. Based on this comparison, we further optimise the algorithm parameters to track individual fire events, for example, the cut of time-delta for separating adjacent but unique fire events.

2.2 Fire type classification

Here we aim to differentiate eight different fire types (Table 1), with some fire types specific to one of the study regions and others more generic. Quality assessment of the fire type classification is based on pre- and post-fire Sentinel-2 pairs. To avoid issues related to class imbalance, we use a stratified random sample of relevant fire types for each region (~100 fires in each class) to assess the accuracy of our classification. Results are presented both on a per fire-object basis and on a per active fire detection basis. Large fires are often better characterised and can therefore more accurately be attributed to a specific fire type, therefore the accuracy for active fire detections (closely related to carbon emissions) is often higher than that of individual events (including many small

fires). In the next session we provide an initial assessment of our capability to separate forest from deforestation fires in Brazil, the first two fire types in Table 1.

Table 1: Fire types by study region.

Fire type	Study region	Tree cover fraction (%)
Evergreen broadleaf Forest fires	Brazil	≥50%
Deforestation fires	Brazil	≥50%
Boreal forest ground fires	Russia	≥50%
Boreal forest crown fires	Russia	≥50%
Woodland fires	Africa	≥50%
Small clearing and agricultural fires	Brazil, Africa, Russia	≥50%
Savannah and grassland fires	Brazil, Africa, Russia	<50%
Cropland burning	Brazil, Africa, Russia	<50%

Separating forest from deforestation fires in Brazil

We assessed the accuracy at which we can separate deforestation from understorey forest fires, two key Amazon fire types associated to forest degradation (Table 2 and Figure 1). Because of the class imbalance, we took a stratified random sample of 100 deforestation and 100 understorey fires across the South American domain in 2019. We focused on fires that started in August, to avoid issues of cloud cover, and used pre- and post-fire Sentinel-2 10m resolution images to interpret the reference fire type. In total, this resulted in a reference set of 163 fires across 110 image pairs, with 37 fires excluded due to cloud cover in either of the image pairs or lack of evidence of burning. Overall, the accuracy of fire type classification improved with fire size, highlighted by an overall accuracy of 67% for fire events and 82% for active fire detections (large fires include more active fire detections; Table 1). The largest difference in accuracy was observed for forest fires, with 58% Producer's accuracy (reflecting omission error) for fire events increasing to 88% Producer's accuracy for active fire detections, likely indicating a more skewed distribution of fire size and associated fire detections compared to deforestation fires. Deforestation fire classification was more stable, with 65% User's and 77% Producer's accuracy for fire events, and 82% User's and 70% Producer's accuracy for fire detections.

Table 2: Accuracy assessment based on 100 deforestation and 100 Amazon forest fires.

The algorithm accurately separated most deforestation from understory forest fires. (a) Accuracy assessment of fire events and (b) accuracy assessment of active fire detections.

a) Fire events		Reference data			
		Deforestation	Forest	Total	User's Accuracy
Classification data	Deforestation	75	21	96	78%
	Forest	44	54	68	55%
	Total	119	75	194	
	Producer's accuracy	63%	72%		
	Overall Accuracy = 66%				
b) Fire detections		Reference data			
		Deforestation	Forest	Total	User's Accuracy
	Deforestation	4,309	667	4,976	87%

Classification data	Forest	1,721	22,997	24,718	93%
	Total	6,030	23,664	29,694	
	Producer's accuracy	71%	87%		
	Overall Accuracy = 92%				

Figure 1: Example highlighting how fire type can be interpreted from 10-m resolution pre- and post-fire Sentinel-2 image pairs.

(a) Deforestation before fire; (b) Deforestation after fire; (c) Mixed forest and deforestation fire before (classified as forest fire)); (d) Mixed forest and deforestation fire (classified as forest fire); (e) Forest fire before (classified as forest fire); (f) Forest fire after (classified as forest fire)

2.3 Burned area estimates

To translate 'fire polygons' to fire emissions we quantify the burned area associated with each fire object. As can be seen in Figure 1, the 550 m (0.005º) spatial resolution of our approach can result in an overestimate of burned area for e.g., deforestation fires that often occur at smaller scales. In contrast, fast moving grassland and savannah fires often burn significant areas not captured with the three daily (1:30 am, 1:30 pm, and 10:00 pm) active fire observations. We therefore developed a strategy to scale burned area with large scaling factors (>1) required for open cover types and small scaling factors (<1) for other fire types, like deforestation fires. Here we assess the quality of these scaled burned area estimates by comparison to Sentinel-2 burned area estimates for 2020 using two different approaches. First, for large forest fires we expect that our approach will provide a close match to the reference burned area data and we therefore assess the quality of burned area estimates on a per-event basis using standard statistical metrics (slope, r^2, RMSE). In contrast, for open cover types we aim to quantify burned area at larger scales, in this case we take various statistical samples (e.g., 1, 10, 20, 50 fire events) and assess how representative these are for the reference burned area (slope, r^2, RMSE). For both approaches we provide standard metrics of quality assessment (User's/Producer's accuracy, precision and recall, and DICE coefficient) at relevant spatial scales.

To create the reference burned area dataset we use the approach developed by Roteta et al. (2021) and a random stratified sample of 2ºx2º Sentinel-2 tiles to map burned area and associated fire type as outlined in the ATBDv1. We stratify our sample such that each region includes 20 2ºx2º tiles including a representative sample of fire types.

3 Fuel loads, moisture content, and fuel consumption

3.1 Conducted calibration/validation activities in PVRv1

Within Sense4Fire, two approaches are developed to estimate fuel loads. The first approach is a comprehensive but still simple empirical model of ecosystem biomass and fuel dynamics (hereinafter referred as **fuel model**) that is solely driven by satellite products and can be constrained by various satellite and ground observations. The second approach is a **machine learning model** to estimate fuel loads by combining the fuel load information from the North American Wildland Fuel Database with satellite datasets. Combustion completeness and fuel consumption are estimated within the fuel model based on its own estimates of fuel loads or by using the estimated fuel loads from the machine learning model as input. Details of both approaches are presented in ATBDv1 (sections 4.3 and 4.4 of ATBDv1). In this PVR, first calibration and validation results for the first approach – the fuel model – are presented. Specifically, calibration and validation tests were performed for the estimation of canopy height (section 4.3.2 of ATBDv1) and tree biomass components (section 4.3.3 of ATBDv1) for the Amazon study area. Further calibration and validation tests and applications to other study areas are foreseen for version 2 of the ATBD and PVR.

The following datasets were used as input into the fuel model:

- LAI from Sentinel-3 OLCI and Proba-V Version 1.1 (Fuster et al., 2020) were used at the original resolution of 333 m and 10-daily product. The LAI ranges from January 2014 to October 2021 (281 observations, 36 observations per full year). Mean LAI was then computed as the average across all observations.
- The fractional coverage of trees (ftree) and herbaceous vegetation (fherb) were derived from the ESA CCI land cover product at a resolution of 300 m. The dataset was resampled using the nearest neighbour method to the resolution of the LAI data.

The following datasets were used for the calibration and validation of canopy height and biomass components of the fuel model:

- The map of forest canopy height from Potapov et al. (2021) combines estimates of canopy height from the GEDI space-borne Lidar with observations from Landsat to produce a global map of forest canopy height at 30 m spatial resolution. To correspond with the LAI data, the dataset was resampled to the same spatial resolution as the LAI data calculating the mean value and then matched to the LAI pixel grid using nearest neighbour interpolation.
- The ESA CCI Biomass map was used for the years 2017 and 2018 (Santoro et al., 2021). The spatial resolution of 100 m of this dataset was resampled to the resolution of the LAI data using nearest-neighbour resampling.
- The Biomass And Allometry Database (BAAD) (Falster et al., 2015) compiles tree-level observations of different biomass components such as the total mass of stems and branches (variable m.st including hardwood, sapwood and bark), mass of branches (variable m.br), mass of leaves (m.lf), total above ground mass (m.so) as well as total plant height (h.t). We estimated stem mass as the difference between m.st and m.br. The estimated biomass per area (kg m^{-2}) was calculated by dividing the mass (kg) with the projected crown area (variable a.cp, m^2).
- Ku-band Vegetation Optical Depth (Ku-VOD) from the VODCA dataset (Moesinger et al., 2020) was used in initial model tests. VOD from other wavelengths will be tested in the calibration exercises for PVRv2.

For the calibration and validation of the height and allometry modules of the fuel model for the Amazon study regions, 10,000 grid cells from the spatial Earth observation datasets were randomly sampled (Figure 2: Overview of randomly sampled points within the Amazon study area for the calibration and validation exercises of the fuel model in PVRv1.Figure 2).

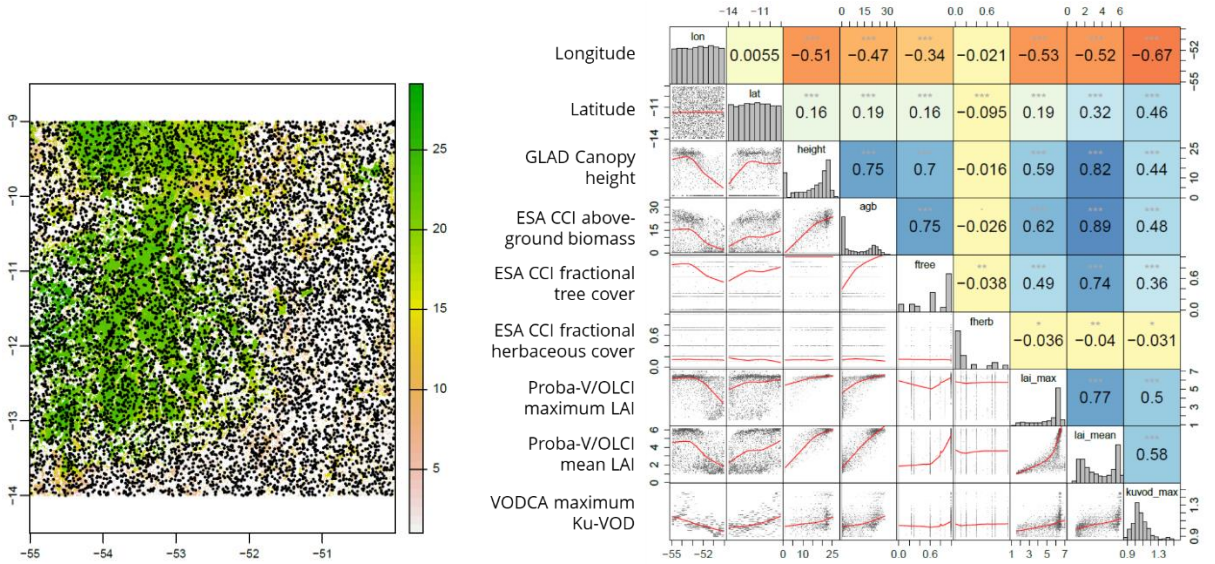

Figure 2: Overview of randomly sampled points within the Amazon study area for the calibration and validation exercises of the fuel model in PVRv1.

(left) Map of canopy height (m) from the GEDI/Landsat-based product with sampled points (black dots). (right) Correlation matrix of the sampled values for canopy height (height), above-ground biomass (agb), mean fractional tree cover (ftree), mean fractional herbaceous cover (fherb), maximum LAI (lai_max), mean LAI (lai_mean), and maximum Ku-VOD (kuvod_max). Numbers in the upper triangle are Spearman correlation coefficients.

3.2 Model selection and validation for canopy height

The computation of canopy height in the fuel model is based on a regression between the predictor variables mean LAI (LAI_{mean}) and fractional tree cover (f_{tree}) and the target variable canopy height H (section 4.3.2 of ATBDv1). The target variable for canopy height is taken from the GEDI/Landsat-based canopy height product (Potapov et al., 2021). Several regression models were tested to predict canopy height (Table 3). Based on the correlation analysis shown in **Fehler! Verweisquelle konnte nicht gefunden werden.**, first linear regression models with one predictor based on either maximum LAI, mean LAI (M1 and M2), or f_{tree} (M3) were tested. LAI_{max} and f_{tree} are insufficient predictors of canopy height and Model 2 based on LAI_{mean} achieved the best performance (Table 3). We then combined LAI_{mean} and f_{tree} in three further regression models that account for non-linear relationships: Model 4 is a Generalised Additive Model (GAM), Model 5 is multi-variate linear regression with LAI_{mean} included as quadratic term, and Model 6 is a random forest. The GAM resulted in a slightly better performance than the other two models, and the random forest and Model 5 achieved similar results (Table 3).

Table 3: Performance statistics of six regression models to estimate canopy height from mean or maximum LAI and fractional tree cover.

Correlation and root mean squared error (RMSE) between canopy height from the GEDI/Landsat-based product and the regression model. Akaike's Information Criterion (AIC).

Model	Correlation	RMSE (m)	AIC
M1) $H = a \times LAI_{max} + b$	0.58	6.69	27266
M2) $H = a \times LAI_{mean} + b$	0.91	3.48	21662
M3) $H = a \times f_{tree} + b$	0.80	4.89	24422

M4) $[GAM]\ H = s(LAI_{mean}) + s(f_{tree})$	0.92	3.24	20954
M5) $H = h1 \times LAI_{mean}^2 + h2 \times f_{tree} + h3$	0.91	3.31	21302
M6) $[RF]\ H = RF(LAI_{mean}, f_{tree})$	0.91	3.33	--

Based on those results, we then select the model to be applied within the fuel model. Akaike's Information Criterion (AIC) suggests that the GAM (Model 4) should be selected because it achieved the lowest AIC value. However, we decided to use Model 5 within the fuel model because the GAM was not strikingly better and Model 5 additionally has the advantage that the three parameters can be simply recalibrated within the entire framework of the fuel model or during applications to other study areas. The estimated canopy height from Model 5 and the reference canopy height from GLAD are compared in Figure 3. This analysis will be repeated when the fuel model will be applied to other study areas in order to ensure consistency in the estimated canopy heights.

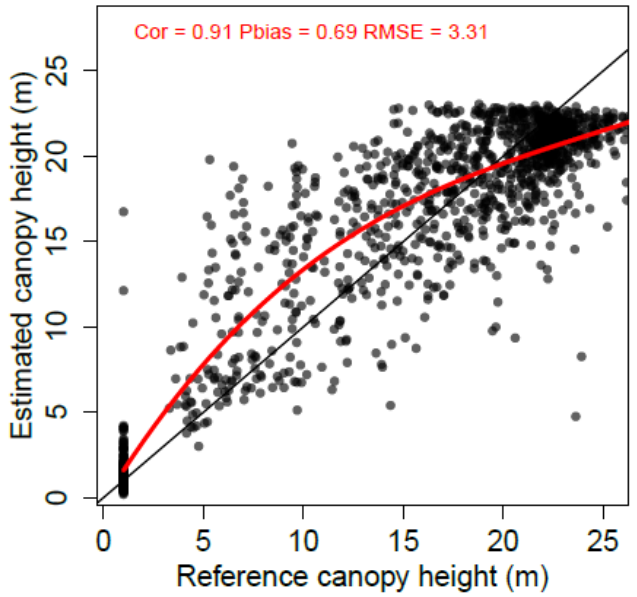

Figure 3: Scatterplot of estimated canopy height against the reference canopy height from the GEDI/Landsat-based on the regression Model M5.

Model 5 was the applied to the entire Amazon study area and compared with the full spatial distribution of the GEDI/Landsat-based canopy height dataset (Figure 4). Both maps show a strong agreement but canopy height is slightly under- or overestimated in certain parts of the study area. The error between the estimated canopy height and canopy height dataset is on average 0.02 m and ranges between -4.6 and 6.1 m in 90% of all grid cells.

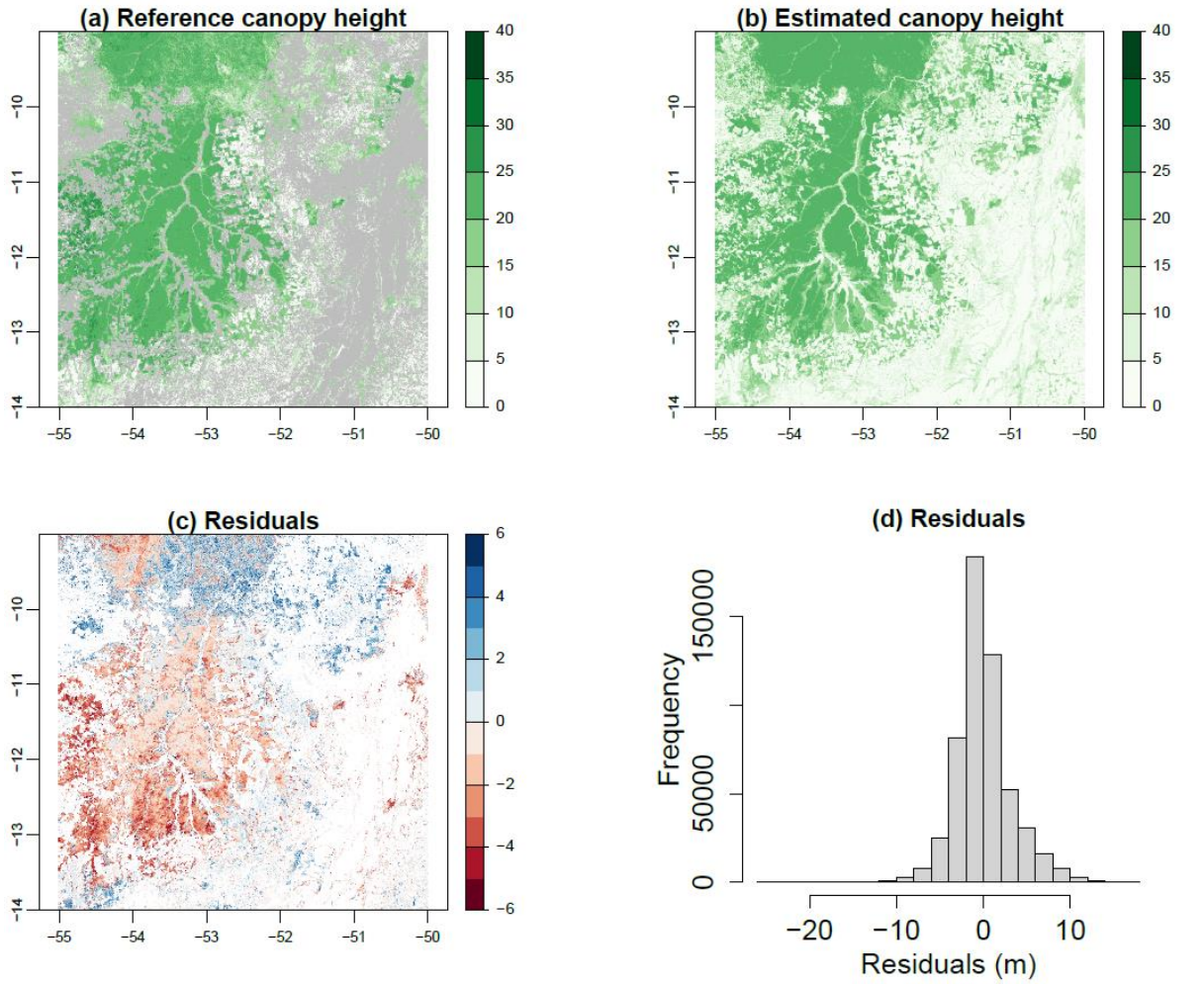

Figure 4: Comparison of canopy height for the Amazon study region.

(a) Reference canopy height map from the GEDI/Landsat-based product. Grey areas are without tree cover according to the canopy height dataset. (b) Canopy height as estimated from mean long-term LAI and fractional tree cover using model M5. (c) Difference map and (d) scatterplot for test data points within the study region that were not used for model calibration.

3.3 Calibration of biomass components against BAAD data

The estimated tree canopy height is used in the fuel model to estimate the biomass of tree stems, branches and leaves based on allometric relationships (section 4.3.3 of ATBDv1). The parameters *a1* to *a6* of these allometric relationships are calibrated against the BAAD measurements. This calibration is independent of the study region and was conducted for all entries in BAAD. The calibration approaches uses a cost function based on the Kling-Gupta efficiency and a genetic optimisation algorithm as described in section 4.3.10 of ATBDv1. To calibrate the parameters of the allometric relationships, we use the measured total tree height from BAAD as input to the allometry module of the fuel model. Thereby, we assume that the phenology status of the leaves is 1, i.e. all measured trees in BAAD are at full seasonal leaf cover. We then compute the total above-ground biomass, the biomass of wood, stem, branches and leaves. The cost function is then computed jointly against the corresponding measurements from BAAD.

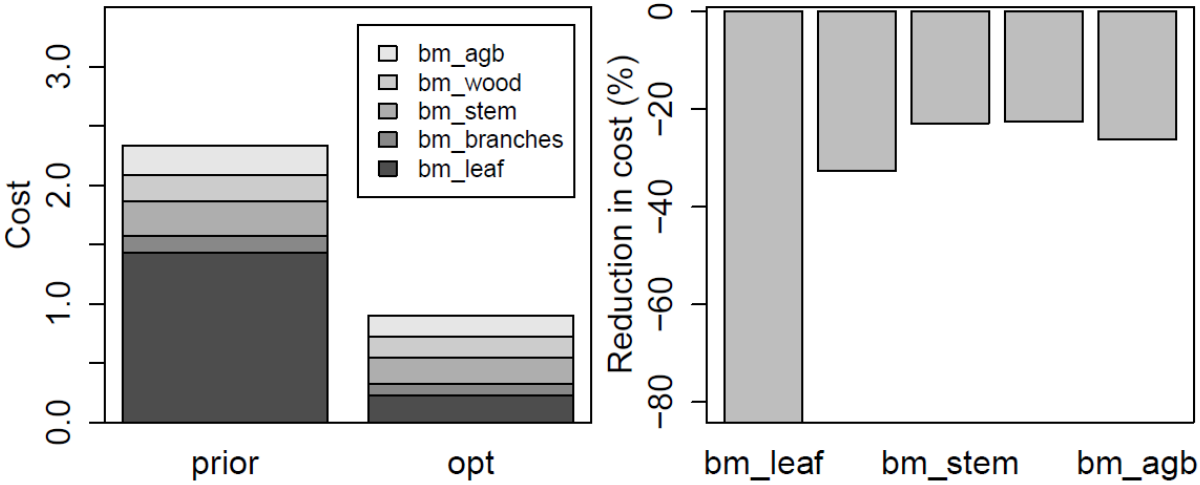

Figure 5: Comparison of the cost of the fuel model prior and after calibration against the BAAD data of total above-ground biomass (BMagb), woody, stem and branches biomass (BMwood = BMstem + BMbranches), and leaf biomass (BMleaf).

The change of the cost function between the prior and the optimised parameter set is shown in Figure 5. Prior to calibration, the cost was dominated by the error in leaf biomass. After calibration, the cost was reduced for all biomass components. The corresponding scatterplots of the calibration results are shown for leaf, branches, woody and total biomass in Figure 6. The allometry model provides an acceptable fit to all biomass components with medium to high correlations and percent biases <= 9%. The lowest performance is thereby achieved in the estimation of leaf biomass. The high scatter in the biomass components for leaves and branches originates from the use of all BAAD observations to derive a prior parameter set that is acceptable for applications in different ecosystems. For the application of the allometry module to specific study regions, we will select from BAAD only observations from tree species that are comparable to species in a study region. Those regional adaptations will be considered in PVRv2.

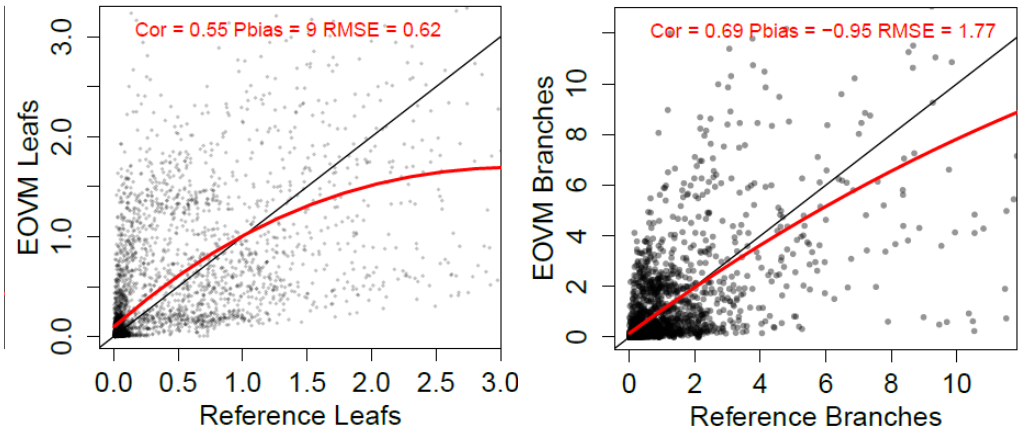

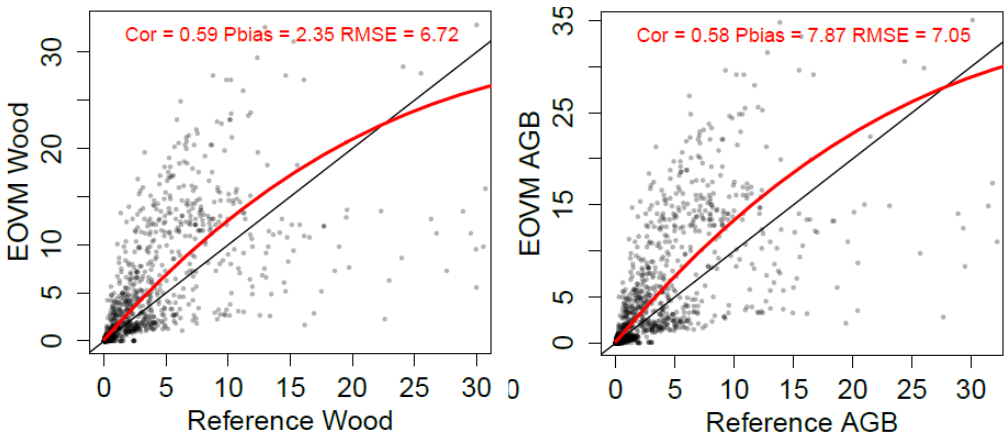

Figure 6: Scatterplots of estimated biomass (kg m^{-2}) compartments from the fuel model (y-axis) against measurements of the BAAD database (x-axis) after optimisation for leaf (upper left), branches (upper right), total wood (lower left), and total AGB (lower right).

3.4 Calibration/validation of biomass components for the Amazon region

In a next step, the biomass of fuel model is calibrated and validated for the Amazon study area. The total woody biomass from the ESA CCI biomass map is used as target variable for the calibration of the model parameters *a1* to *a6* and canopy height from the GEDI/Landsat-based product is used as input to the fuel model. As the ESA CCI biomass map can only provide constrain on total woody biomass but does not contain information on leaf, stem or branches biomass, the calibration approach will be not informed about how different biomass components contribute to total woody biomass. For this reason, we perform a joint calibration against total woody biomass from the ESA CCI map and against the stem, branches and leaf biomass from BAAD. To achieve such a calibration, we combine both datasets, i.e. the dataset first includes 10,000 observations from the randomly sampled grid cells shown in Figure 2**Fehler! Verweisquelle konnte nicht gefunden werden.** (only for total woody biomass, values for all other components are missing) and then 928 observations from BAAD (only stem, branches, leaf and total woody + leaf biomass but not total woody biomass). The cost function then includes five variables.

The results of the fuel model from this joint calibration are shown for stem biomass (based on BAAD) and total woody biomass (based on ESA CCI biomass) in Figure 7. The model performance improved for both datasets (and also for leaf and branch biomass) after calibration. These results demonstrate that the fuel model can make a best estimate for different biomass components and total woody biomass that is constrained by both the satellite-based biomass map and a database of tree measurements.

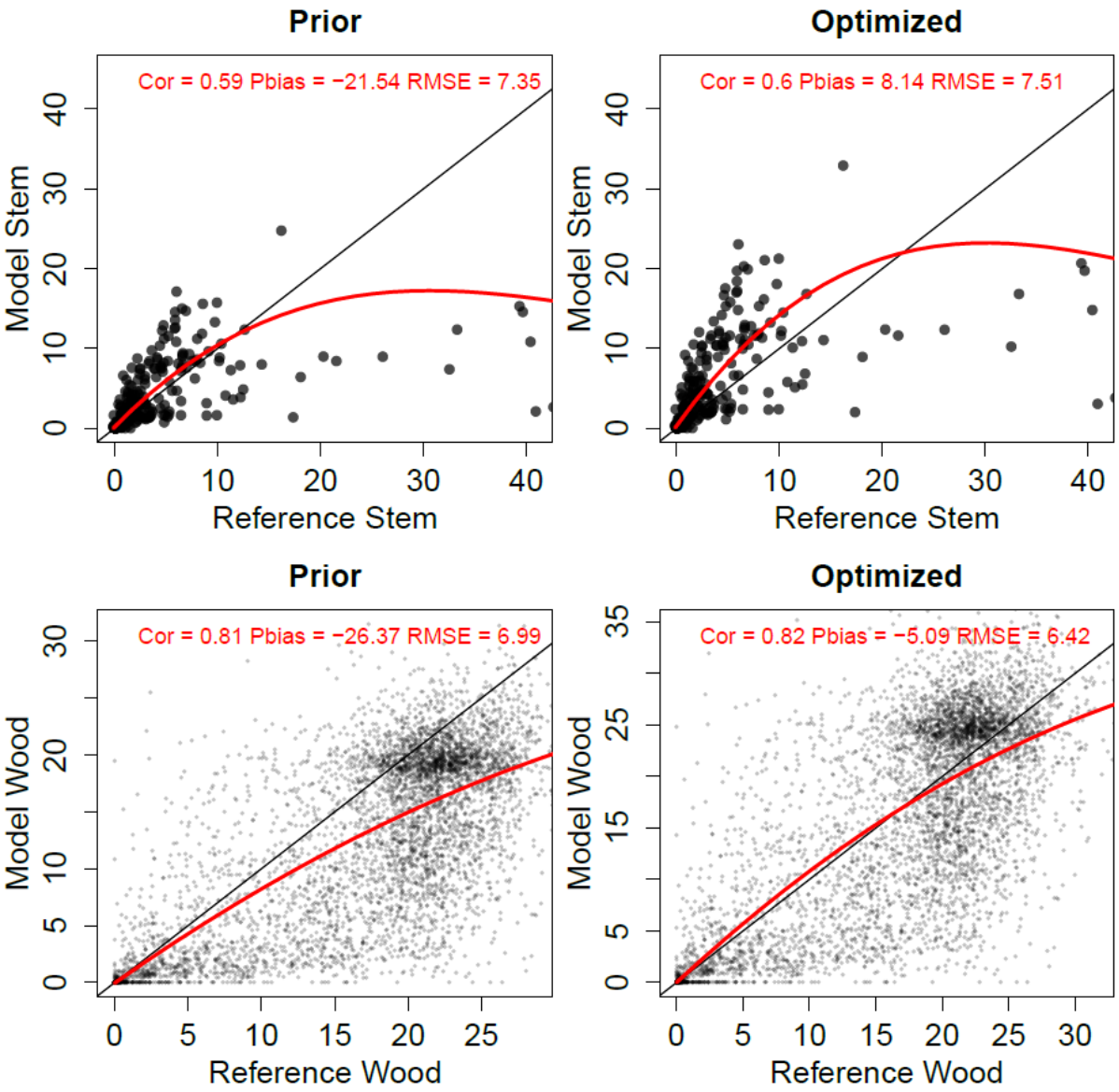

Figure 7: Results of a joint calibration of the fuel model against stem biomass from the BAAD database (upper panel) and against total woody biomass from the ESA CCI biomass map in the Amazon study region (lower panel).

Units are in kg m^{-2}. The results show that estimates of biomass compartments can be achieved that are consistent with the BAAD database and the ESA CCI biomass map.

The fuel model represents biomass as a function of tree height. The tree height-biomass relationships from the fuel model and the relationships that can be derived from BAAD, and from the canopy height and biomass maps for the Amazon study area are compared in **Fehler! Verweisquelle konnte nicht gefunden werden.**. The fuel model both before and after calibration resembles well the relationship found in BAAD. After calibration, the fuel model also better captures high values of biomass in the Amazon study region.

An interesting pattern is, however, the very different relationship between height and woody biomass that can be derived from the two satellite datasets (i.e. the GEDI/Landsat-based canopy height and ESA CCI biomass map). ESA CCI biomass shows a stronger increase at low canopy height and canopy height shows little sensitivity to biomass at high

biomass. This relationship is not supported by the BAAD measurements and suggests inconsistency between both datasets.

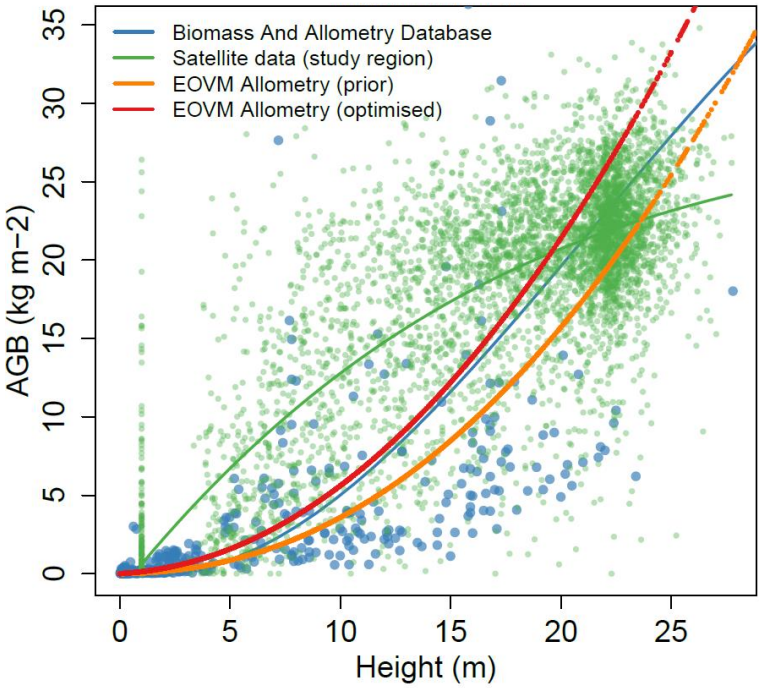

Figure 8 : Relationship between tree height and total above-ground woody biomass from the BAAD database (blue, all available observations), and for the Amazon study region from the fit between the GEDI/Landsat canopy height dataset and ESA CCI above-ground biomass (green, 10,000 sampled grid cells), and from the fuel model before and after calibration (orange and red).

The calibrated parameters of the fuel model are then applied to the entire Amazon study area and the estimated woody biomass is compared with the ESA CCI biomass map. Thereby, we first estimate canopy height from mean LAI and fractional tree cover by using the regression model M5 (Table 3) and compute then the biomass components and total woody biomass (Figure 9). We additionally compute the biomass components using the canopy height map as alternative input dataset (Figure 10). Based on mean LAI and fractional tree cover as input the fuel model captures well the spatial patterns of total woody biomass with a spatial correlation of 0.93 and a RMSE of 3.93 kg m^{-2} (Figure 9 d). The difference between estimated and ESA CCI woody biomass ranges between -8.5 and 3.7 kg m^{-2} in 90% of all grid cells.

Interestingly, the agreement of the estimated woody biomass with the ESA CCI biomass is better when tree height is estimated from mean LAI and fractional tree cover than in the case when the GEDI/Landsat-based canopy height dataset is used as input (Figure 10). In this case, the RMSE is clearly higher and more spatial clusters with a clear under- or overestimation of woody biomass are present (Figure 10 c). These results demonstrate that the use of mean LAI and fractional tree cover as predictors for tree height in the fuel model are a more appropriate choice than the direct use of the canopy height datasets to achieve consistency between multiple satellite products.

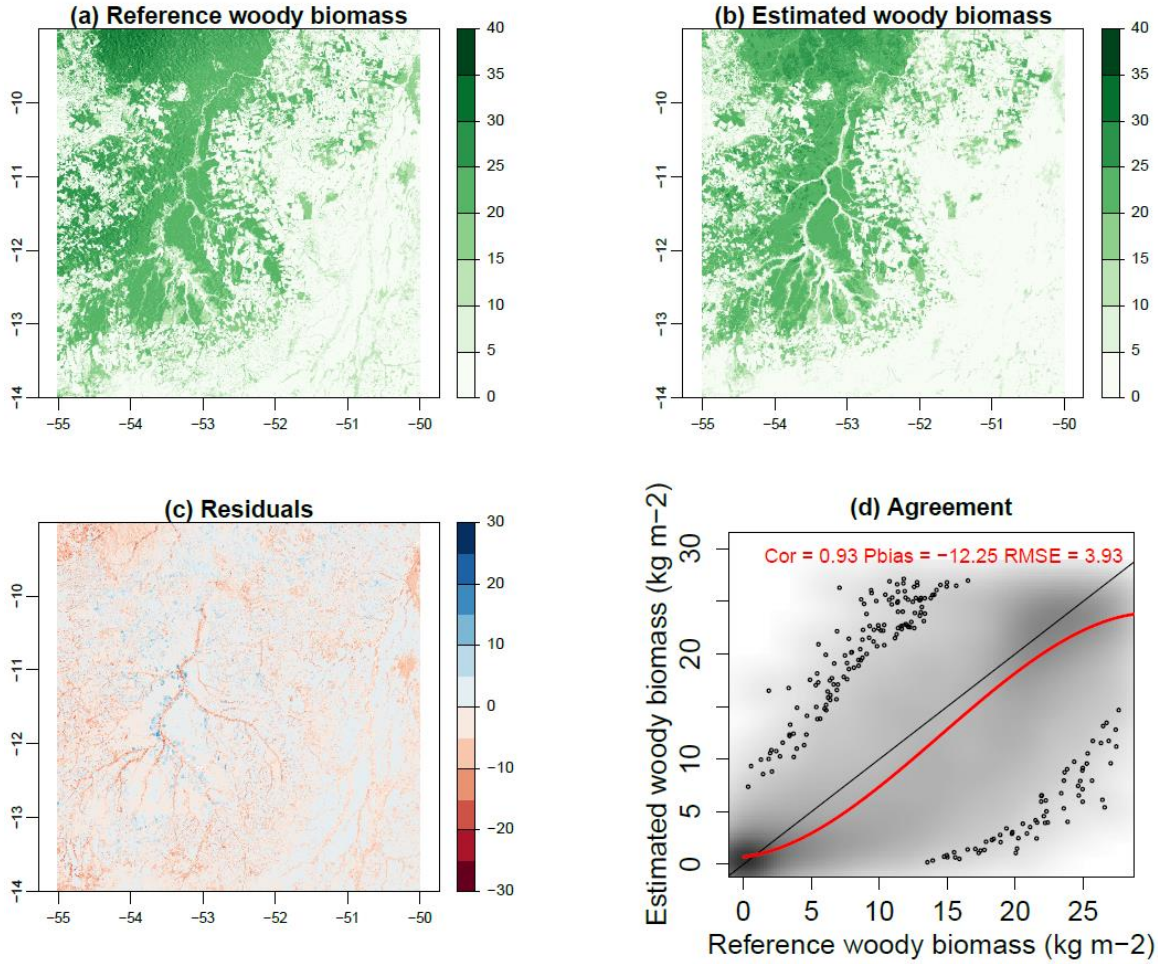

Figure 9: Comparison of woody above-ground biomass (kg m^{-2}) for the Amazon study region.

(a) Reference biomass map from the ESA CCI biomass product (year 2017). (b) Woody biomass as estimated with the fuel model using mean long-term LAI and fractional tree cover to predict tree height. (c) Difference map and (d) scatterplot.

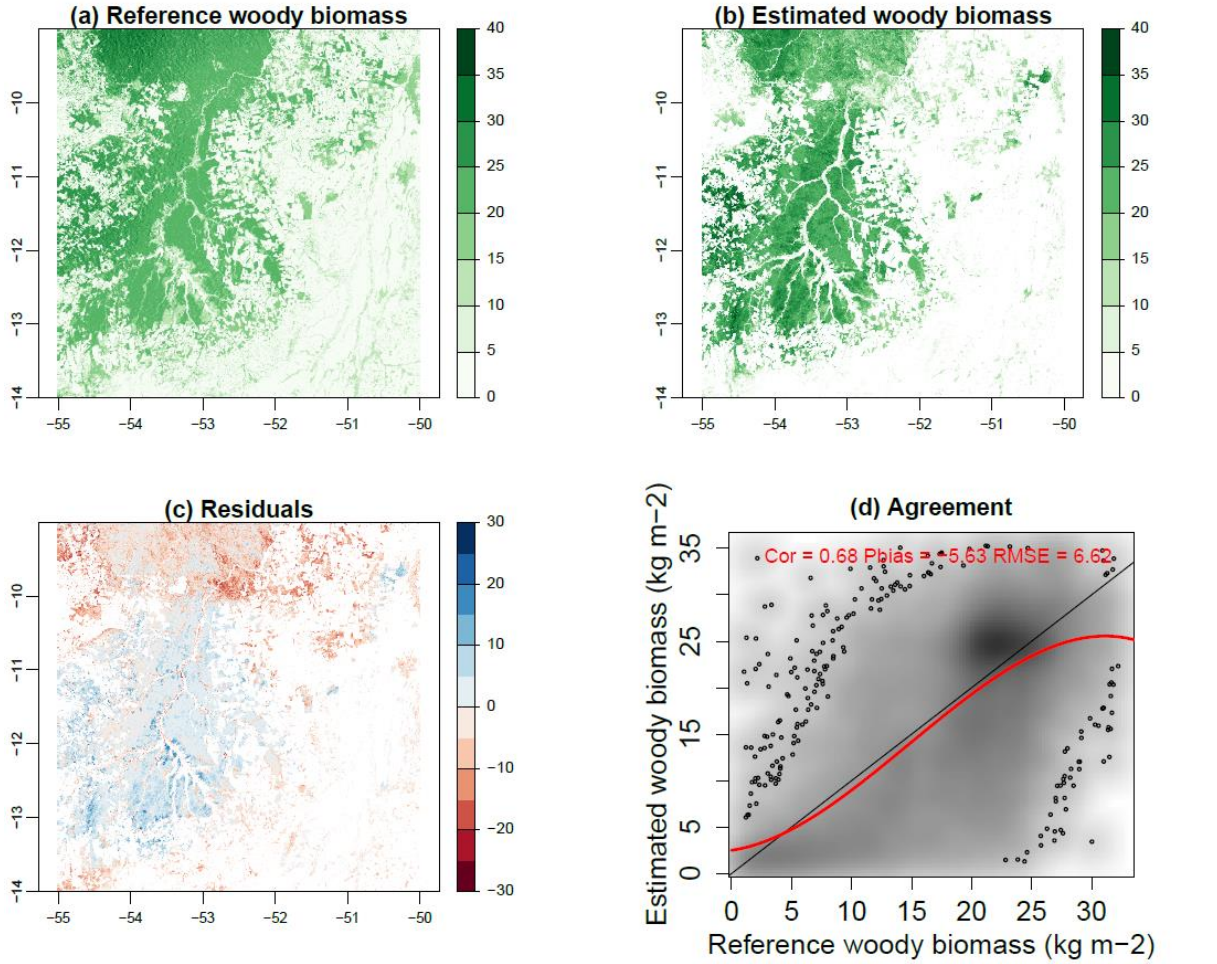

Figure 10: The same as in Figure 7 but by using the GEDI/Landsat-based canopy height map as direct input into the fuel model to compute biomass components.

3.5 Planned calibration/validation activities for PVRv2

The previous results demonstrate that the fuel model can be successfully calibrated against diverse datasets (Earth observation and field measurements) to estimate different vegetation biomass components that are to a high degree in agreement with the ESA CCI biomass map. Further modules of the fuel model, specifically for herbaceous biomass, litter and surface fuel production, fuel moisture, combustion completeness and fuel consumption will be calibrated and validated for version 2 of the PVR. PVRv2 will also contain calibration/validation results for the other study areas in Sense4Fire. Specifically, we plan the following calibration/validation activities:

Retrievals of forest canopy height from GEDI will be directly used to calibrate and validate tree height in the fuel model. This comparison will allow a thorough understanding of the inconsistency found between the GEDI/Landsat-based canopy height and ESA CCI biomass maps.

The computation of live-fuel moisture content in the fuel model will be calibrated and validated against measurements from the Globe-LFMC database (Yebra et al., 2019). Additionally, we plan to test the use of microwave satellite datasets (Sentinel-1 and passive microwave VODCA dataset) to estimate LFMC. Therefore, we will test VOD-derived

estimates of LFMC (Forkel et al., 2022) within the fuel model and will explore a modification of the approach by Wang et al. (2019) to estimate LFMC from Sentinel-1.

The estimated biomass components and vegetation water content in the fuel model affect the computed vegetation optical depth (VOD). Hence the fuel model will be additionally calibrated and compared against short-wavelength VOD (e.g. Ku and X-band VOD from the VODCA dataset) and L-band VOD time series from SMOS and SMAP.

Several parameters of the fuel model such as specific leaf area (*sla*), woody moisture content, the fraction of small branches f_{sb}, the decomposition rates for litter, fine and coarse woody debris (k_i), and for the conversion factor *cf* for fuel consumption to FRE will be calibrated based on values found in the literature. In addition the TRY plant trait database (Kattge et al., 2011) will be investigated to obtain plausible values for some parameters.

Model parameters that control fuel consumption will be calibrated based on reported values on combustion completeness and fuel consumption from the fuel consumption database (van Leeuwen et al., 2014). The fuel model will be also calibrated and validated based on satellite observations of fire radiative energy for a selection of fire events within the study areas.

Finally, estimated of fuel loads and fire emissions of the fuel model will be benchmarked against other large scale integrated datasets or models. Specifically, we plan to compare estimate of fuel loads with the North American Wildland Fuel Database (Prichard et al., 2019) by applying the fuel model to parts of the United States. Estimated fuel loads will be also compared against the global fuelbed map (Pettinari and Chuvieco, 2016). Estimated fuel consumption and fire emissions will be also compared with the model estimates from the CASA model used in the Global Fire Emission Database (van der Werf et al., 2017) for the study regions.

4 Top-down constraints on fire emissions

4.1 Theoretical baseline

Current state-of-the-art satellite observation-based fire emission databases such as GFAS and GFED combine information of burned area and active fire detections with associated radiative power to derive trace gas emissions that are further used for estimating fire total carbon emissions. However, total carbon emission using existing methods are highly uncertain. Fire emissions – and in particular ratios of emissions between various trace gases - also depend on for example the type of vegetation and the hydrological conditions of the vegetation. Such information has now become available from the Sentinel 1-2-3 satellite missions but that information is not yet used to upgrade and improve state-of-the-art fire total carbon emission estimates. The Sense4Fire project aims to bridge this gap.

Satellite-based assessment and evaluation of fire emissions to date have mostly relied on satellite measurements of CO and HCHO. Model simulations of atmospheric chemistry and the atmospheric composition are used to bridge the gap between emissions and satellite observations by using the fire emissions as boundary conditions for simulating the atmospheric chemical composition. Although useful to estimate the continental and global effects of fire emissions, the satellite measurements of CO and HCHO that have been used so far, e.g. based on MOPITT and OMI instruments, are less suitable for detailed regional to local evaluation of emissions due to the need to average satellite data in time and/or space, and the relatively coarse spatial resolution of satellite measurements.

The Sentinel-5p satellite mission (TROPOMI) provides joint measurements of fire-relevant trace-gases CO, HCHO, NO_2, as well as aerosol properties, with unprecedented accuracy and spatial resolution. This opens hitherto unavailable possibilities to assess fire emission estimates. The accuracy and spatial resolution Sentinel-5p trace gas measurements allow for zooming in on much smaller regions, and spatiotemporal averaging is for CO and NO_2 not needed, *i.e.* Sentinel-5p is capable of monitoring individual fire emission plumes on a daily basis. Furthermore, the accuracy also allows for advanced use of trace gas ratios, which provides additional information about the fire process as especially NO_2 and CO emission dependencies differ significantly. The combined focus on NO_2, CO (HCHO) and aerosol parameters (AAI, ALH) thereby allows for better constraining total fire carbon emissions. The emissions of NO_2 and CO (HCHO) depend on different fire characteristics. NO_2 is typically emitted at higher burning temperatures (Zeldovich mechanism), whereas CO (HCHO) emissions are the result of incomplete combustion. Both depend on fuel type and fuel characteristics such as mass and (soil) moisture, but in a different way. The more incomplete the combustion, the more carbon that remains unburned and the less NO_2 emission that are expected. Sentinel-5p trace gas ratios thus can provide information about the burning efficiency and thereby constraining burned and emitted carbon. Aerosol information allows for estimating emission mass determination of plume extents and volumes but also to characterise fire types: more incomplete combustion will result in a larger amount of unburned (scarred) fire material and higher AAI values.

Feeding the Sentinel 1-2-3 based high resolution emission estimates as boundary conditions into the IFS/CAMS model simulations then allows for a detailed comparison with Sentinel-5p data to make optimal use of the information richness of Sentinel-5p data. Sentinels 1-2-3 observe surface characteristics at much higher spatial resolution than Sentinel 5p (~300 metre for Sentinel-3; ~10-60 metre for Sentinel-2 depending on wavelength; 5 metre for Sentinel-1). The Sentinel 1-2-3 observations are then used to quantify fire behaviour, burned area and fuel information and combined to identify fire types and estimated fire emissions (see Sense4Fire ATBD for details). Feeding all the information of the comparison back into the algorithms and data used by the algorithms has the potential to validate and improve emission estimates of these parameters and thereby – via the dependence of emissions on fire characteristics as described above – also improve associated emissions of total carbon.

4.2 Input data

For constraining the emissions top down using Sentinel-5p data the analyses is performed for four regions and time periods defined in Chapter 2 in the ATBDv1.

The Sentinel-5p data being used is tropospheric NO_2, CO total columns, HCHO total columns, the AAI, and the ALH. The accuracy of tropospheric NO_2 and CO is sufficient to be used in a daily basis at the Sentinel-5p spatial resolution.

The short atmospheric lifetime of NO_2 - hours - ensures that local enhancements of NO_2 near fires can almost uniquely be attributed to those fires unless there are non-fire NO_2 sources in the immediate vicinity of the fires. The regions defined in section 1 were chosen such that there are few other sources like cities or industrial activities. Due to its decreasing vertical sensitivity with altitude, the Sentinel-5p NO_2 averaging kernel needs to be applied for the comparison with model simulations. Also, for sufficiently thick aerosol clouds the Sentinel-5p NO_2 quality flag values are lower, indicating that the tropospheric NO_2 date product actually may not have sensed the entire tropospheric column. Depending on the chosen data quality threshold such measurements then may be discarded, even though they still can provide valuable information of the emitted NO_2. Although it is beyond the scope of the Sense4Fire project to explore individual fire plume behaviour, it is explored to some extent whether there is added value in considering such lower quality tropospheric NO_2 measurements.

CO has a much longer atmospheric lifetime (weeks to months) than NO_2, resulting in seasonal changes in background CO levels due to accumulation of widespread emissions and/or advection. These seasonal changes are considered and accounted for in analyses, especially when averaging over longer periods of time as background CO levels vary seasonally. An advantage of Sentinel-5p CO is that its vertical sensitivity is nearly uniform so that to first order the effect of the averaging kernel is limited (even though it is applied).

HCHO has a lifetime more similar to that of NO_2 but due to the lower accuracy of Sentinel-5p HCHO measurements time averaging for HCHO time averaging is required, which limits the possibility to explore HCHO variations on a daily to multi-day basis. Similar to NO_2, the HCHO averaging kernel must be considered for the model comparison.

The AAI – being a qualitative indicator of absorbing aerosols - is used strictly qualitatively for identifying the extent of emission plumes and/or air masses being affected by fire emissions.

The ALH can be used for estimating the height of aerosols. However, the ALH measures a centroid aerosol layer height, not the top of the aerosol layer height. Also, the ALH is more accurate for optically thinner aerosol plumes. This, however, strongly reduces the number of useful ALH observations. For optically thick aerosol plumes the ALH quality flag values are lower, and depending on the chosen quality flag thresholds, may be disregarded. However, for optically thick aerosol plumes the atmospheric oxygen-based cloud top height can be used as a cloud top height proxy [see (de Laat et al., 2020)]. Because of the

reduced capacity to assess aerosol layer heights by standard use of the ALH, the use of cloud top heights for optically thick aerosol plumes as proxy for the ALH is explored. For identifying optically thick aerosol plumes the AAI is used. There is some ambiguity of the Sentinel-5p AAI values to identify optically thick aerosol clouds. For a strict filtering AAI values > 4 are used, but it has been suggested that AAI values > 2 can also be used as long as no bright clouds are present below the aerosol plume (de Laat et al., 2020). In case of the regions and fires considered in Sense4Fire, emission plumes are expected mostly in the boundary layer and/or the lowermost atmosphere (*e.g.* (Val Martin et al., 2010); (Veira et al., 2015); (Rémy et al., 2017)). Hence it is generally not expected that many scenes with clouds below the aerosol plumes occur, but it is something to keep in mind when performing the Sense4Fire analyses.

The IFS/CAMS global atmospheric composition modelling system is used to simulate the atmospheric conditions during the periods and for the regions under consideration (see Chapter 1). The model results serve to bridge the gap between bottom-up emission estimates (Sentinel 1-2-3, GFAS, GFED) and Sentinel-5p observations. GFAS and GFED are the state-of-the-art and widely used and referred to satellite-observation-based fire emission databases (GFAS in near-real-time and GFED as a post-processing data product). As the aim of Sense4Fire is to improve satellite-observation-based fire emission estimates, results should be shown to improve on what are the current fire emission standards. The model results can be compared with Sentinel-5p observations after applying satellite observation operators.

The IFS/CAMS model is using target CY48R1 tropospheric chemistry and aerosol modules. It is driven by ECMWF operational meteorology, and using emissions (including anthropogenic and biogenic) as prepared for the operational model configuration. It is setup to run at an approximately 40 km spatial resolution (T511 reduced gaussian grid), with 137 vertical model levels (approximately 60 layers in the lowest 10 km of the atmosphere). This implies that the horizontal model resolution (0.25 degrees at best, which is approximately 25 km) is much less refined than the Sentinel 1-2-3 data (sub-km scale), emission estimates (km scale) and the Sentinel-5p spatial resolution (3.5x5.5 km at best). This may have a considerable effect on the model-observation comparison, especially as localised sub-model scale non-linear emission plume chemistry may result in changes in atmospheric composition that differ from direct injection of fire emissions at the native model resolution, particularly for short-lived trace gases. This is a well-known phenomenon from for example transport (aviation, shipping, road traffic) but also stationary sources such as power plants. Such impacts traditionally have been mitigated in modelling by applying resolution-dependent correction factors to emission values. To what extent such sub-model-grid processes also play a role for fire emissions is not well established but will be considered within the context of Sense4Fire study and results.

4.3 Methods

To enable constraining fire emission using a top-down approach the following topics need to be addressed to validate this method:

1. analysis of sensitivity to model parameters and model input affecting assessment of fire emissions
2. comparison of model simulations with Sentinel-5p data to derive conclusions on input fire emissions
3. optimising the bottom-up emission estimates based on results above

These topics are evaluated based on the following set of Sentinel-5p parameters relevant for fire emission monitoring:

i. Nitrogen Dioxide (NO_2) tropospheric column
ii. Carbon Monoxide (CO) total column
iii. Formaldehyde (HCHO) total column
iv. Absorbing Aerosol Index (AAI)
v. Aerosol Layer height (ALH)

Note that Sentinel-5p is only capable of measuring the total column amounts of CO, HCHO and tropospheric NO_2. However, the accuracy and precision of Sentinel-5p measurements of CO tropospheric NO_2 is sufficient to allow measuring daily single satellite pixel atmospheric enhancements of both due to fires and near fires. Furthermore, free tropospheric abundances are small most of the time (tropospheric NO_2 and HCHO) and/or free tropospheric abundances vary more slowly (CO) which allows for monitoring single fire emission plumes. For longer lived CO slowly varying background CO levels need to be kept in mind. These include seasonal cycles due to larger scale to regional to continental accumulation of CO in the free troposphere in case of widespread persistent fires such as over the Amazon and equatorial Africa. However, such slow varying background CO levels and especially spatial gradients are well represented in the IFS model. For HCHO the lower Sentinel-5p single pixel accuracy and precision means some averaging is needed, making it less useful for fire monitoring.

Furthermore, the following observed and modelled trace gas enhancement ratios in fire-emission affected regions are explored. Note that these ratios are compared with IFS modelled ratios in which the averaging kernels are taken into account, rather than studying the ratios themselves. By comparing with IFS model results differences in vertical sensitivity is initially irrelevant. However, if needed, the availability of IFS model results allow to explore the sensitivity of analysis results to differences in Sentinel-5p vertical sensitivity for different parameters:

vi. NO_2/CO
vii. HCHO/CO
viii. HCHO/NO_2

Model experiments varying the following model parameters and input data are performed and analysed to identify, characterise, and rank their impact on the model results.

A. model resolution (0.25, 0.5, 1 degree)

B. emissions amounts (GFAS, GFED; variations in emission factors)
C. emission heights
D. diurnal cycle of emissions
E. model chemistry
F. observation filtering selection criteria

The baseline simulation is then compared with Sentinel-5p observations for the Sentinel-5p parameters listed above, taking observation operators into account. This provides understanding on the use of Sentinel-5p satellite observations in the interpretation of emission biases, and in particular understanding on the interpretation of the optimal way to optimise Sentinel 1-2-3 based emissions.

To test the ability to put constraints on each of the parameters (i-viii) a model simulation will be performed and compared with the baseline model simulation to identify where and when results differ, and by how much. The comparison will focus on spatiotemporal variations of selected parameters but also the comparison of probability distribution statistics of selected parameters. Note that other evaluation methods may be defined depending on the results and feedback from consortium members on preliminary results.

The diurnal cycle of emissions is based on fire radiative power climatologies.

4.4 Validation approach

Validation of the Sense4Fires emission estimates can subsequently take place using the IFS/CAMS modelling system. Specifically, the IFS/CAMS reference configuration is run with different variants of the Sentinel 1-2-3 based updated emissions and analysed to identify the best-performing configuration with respect to Sentinel-5p data, taking observation operators into account. The comparison results will then be further analysed by evaluation of differences with Sentinel 1-2-3 based emission parameters such as burned area, fuel type, fuel moisture content, and soil moisture content.

Disagreement is further explored by tracing the disagreement back to specific fires and/or fire locations. The specific emission characteristics of fire emission at the identified location is evaluated, including the results from the sensitivity analyses performed before: given the results of the sensitivity analyses, what is the most likely explanation of the differences found, and do these differences fall within estimated uncertainty limits or are updates of the emissions needed. These findings are then used to update and optimise the Sentinel 1-2-3 emission estimates.

The results of the comparison of IFS/CAMS model simulation with updated Sentinel 1-2-3 emissions and Sentinel-5p observations are evaluated against the uncertainty ranges derived from the model sensitivity tests.

In addition, these results are also evaluated against limitations of the sensitivity analysis. Certain sensitivities may be difficult to capture and/or constrained with the existing IFS/CAMS model setup up. Certain processes may not be captured or resolved at the desired scales, may be difficult to constrain due to limited or missing information and

data, or may be difficult to tailor as a whole (*e.g.* optimise an entire atmospheric chemistry scheme).

Finally, other uncertainties are explored and characterised on a best-effort-basis, for example assumptions about parameters and parameter values *(e.g.* emission factors), observations and methods. This is by no means a simple and straightforward exercise and may result in an incomplete analysis but it is important to identify how fire emission estimates can be further improved.

4.5 Example results

Figure 11 shows a comparison of IFS simulated tropospheric NO_2 columns and Sentinel - 5p for the GFAS emissions on 10 September 2020. The comparison is shown for a larger region over the Amazon than originally defined within the Sense4Fire project (black box in the plots).

The scatter plot shows that there is a reasonable agreement between simulated and observed tropospheric NO_2 columns but that there are some fire hot spots where IFS overestimates tropospheric NO_2.

These data can also be accumulated into a probability distribution as shown in Figure 12, in this case for the originally defined Amazon regions (black box in Figure 11) but for all data in August and September 2020. Results reveal a fair agreement between modelled and observed tropospheric NO_2 columns but again some significant overestimation of NO_2 emissions. These overestimations of tropospheric NO_2 columns generally worsen for the S^4F emissions (Cardiff) compared to the GFAS emissions.

Figure 13 shows a similar probability distribution but for carbon monoxide (CO). Here, the S^4F emissions significantly improve the comparison between model simulations and observations compared to the simulations with GFAS emissions. The comparison with GFAS emissions reveals a significant low bias (GFAS emissions too small) by 40% or more. With the S^4F emissions this bias is significantly reduced (20% or less) and differences fall within the data spread.

Note that results shown here are for illustration purposes as analyses are ongoing and results expected to improve, to be extended, to be expanded, and to be refined.

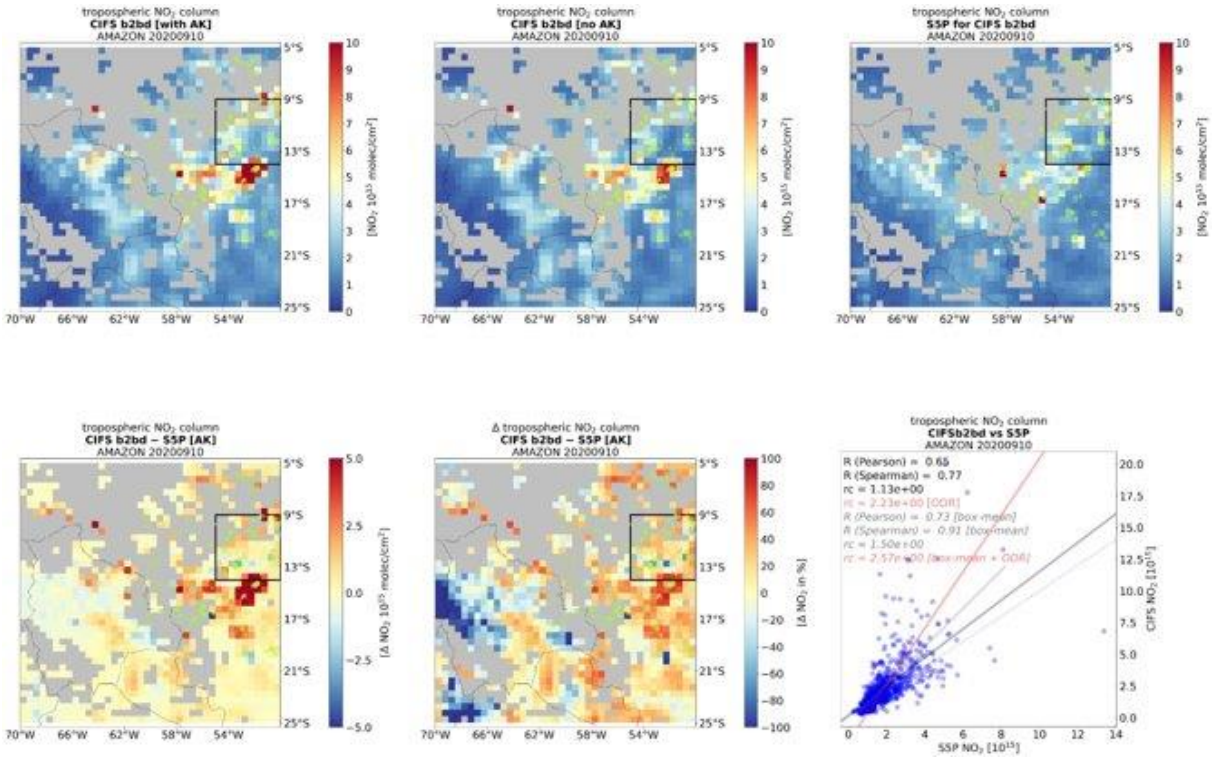

Figure 11: Comparison of IFS simulated tropospheric NO_2 columns with GFAS emissions (B2BD)

Upper left with applying the Sentinel-5p tropospheric NO_2 columns averaging kernel, upper middle without applying the averaging kernel) and Sentinel-5p tropospheric NO_2 column measurements (upper right). The differences between IFS and Sentinel-5p tropospheric NO_2 columns are shown in the lower left plot (absolute differences) and lower middle plot (relative differences). The lower right plots shows the scatter plot and several statistics and linear fits. Results are just for illustration purposes.

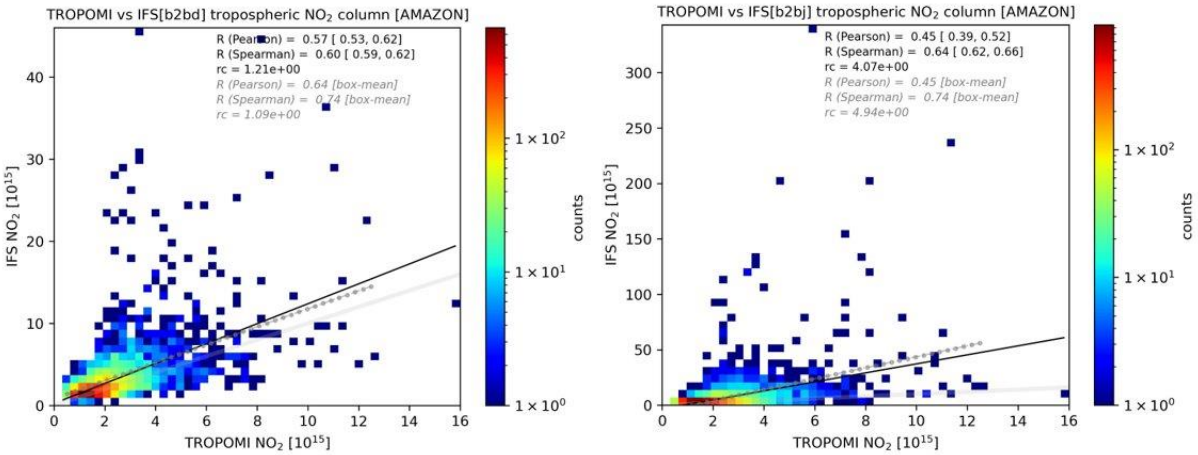

Figure 12: Probability distribution IFS simulated and Sentinel-5p observed tropospheric NO_2 columns for the originally selected S[4]F Amazon region.

Left plot shows the comparison for GFAS emissions (B2BD), right plot for S[4]F (Cardiff) emissions (B2BJ). Indicated are also some statistics of the comparison and linear regression fits. Results are for illustration purposes.

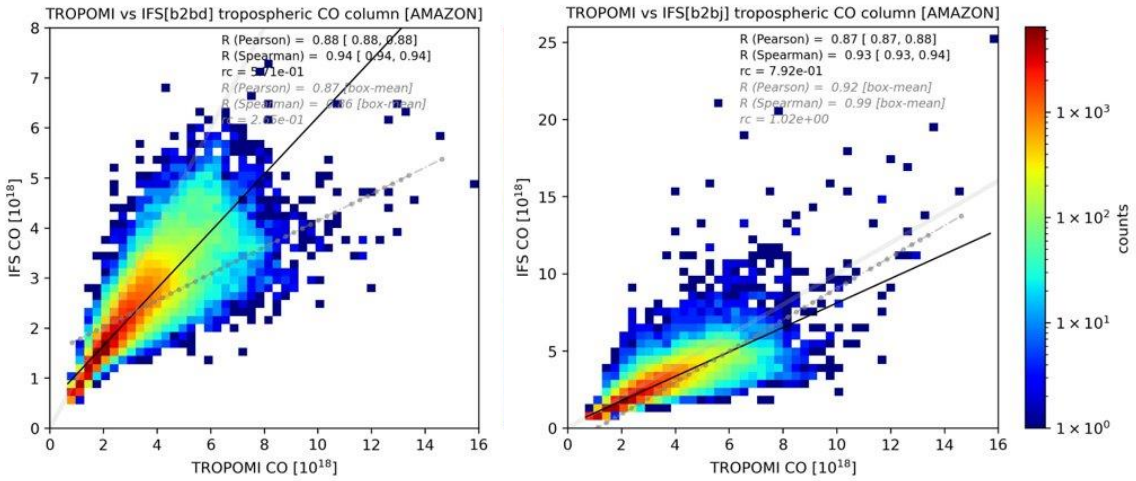

Figure 13: As Figure 12 but for carbon monoxide total columns and for the larger Amazon region shown in Figure 11.

Left plot shows the comparison for GFAS emissions (B2BD), right plot for S^{4}F (Cardiff) emissions (B2BJ). Indicated are also some statistics of the comparison and linear regression fits. There is a thin grey line indicating the 1:1 line (visualisation to be improved). Results are for illustration purposes.

4.6 Limitations and gap analysis

The validation results are analysed from a data product improvement framework. They can be of use immediately to improve data products and algorithms in the Sense4Fire data production chain. These improvements may be immediately implemented and used within the project in an iterative process. More fundamental limitations, which cannot be resolved within the Sense4Fire project duration, will also be identified and described in terms of their complexity, and implementation requirements. To resolve these aspects a project extension or follow-up project would be required. Finally, some of the improvements needed may fall outside of the project consortium capacity – for instance fundamental model refinement or improved quality of satellite data products – which would result in recommendations for additional research and/or development. Combined, the validation analysis and evaluation results should provide clear pathways towards improvement.

References

Andela, N., Morton, D. C., Giglio, L., Paugam, R., Chen, Y., Hantson, S., Van Der Werf, G. R., and Randerson, J. T.: The Global Fire Atlas of individual fire size, duration, speed and direction, Earth Syst. Sci. Data, 11, 529–552, 2019.

Barrett, K., Baxter, R., Kukavskaya, E., Balzter, H., Shvetsov, E., and Buryak, L.: Postfire recruitment failure in Scots pine forests of southern Siberia, Remote Sens. Environ., 237, 111539, https://doi.org/10.1016/j.rse.2019.111539, 2020.

Falster, D. S., Duursma, R. A., Ishihara, M. I., Barneche, D. R., FitzJohn, R. G., Vårhammar, A., Aiba, M., Ando, M., Anten, N., Aspinwall, M. J., Baltzer, J. L., Baraloto, C., Battaglia, M., Battles, J. J., Bond-Lamberty, B., van Breugel, M., Camac, J., Claveau, Y., Coll, L., Dannoura, M., Delagrange, S., Domec, J.-C., Fatemi, F., Feng, W., Gargaglione, V., Goto, Y., Hagihara, A., Hall, J. S., Hamilton, S., Harja, D., Hiura, T., Holdaway, R., Hutley, L. S., Ichie, T., Jokela, E. J., Kantola, A., Kelly, J. W. G., Kenzo, T., King, D., Kloeppel, B. D.,

Kohyama, T., Komiyama, A., Laclau, J.-P., Lusk, C. H., Maguire, D. A., le Maire, G., Mäkelä, A., Markesteijn, L., Marshall, J., McCulloh, K., Miyata, I., Mokany, K., Mori, S., Myster, R. W., Nagano, M., Naidu, S. L., Nouvellon, Y., O'Grady, A. P., O'Hara, K. L., Ohtsuka, T., Osada, N., Osunkoya, O. O., Peri, P. L., Petritan, A. M., Poorter, L., Portsmuth, A., Potvin, C., Ransijn, J., Reid, D., Ribeiro, S. C., Roberts, S. D., Rodríguez, R., Saldaña-Acosta, A., Santa-Regina, I., Sasa, K., Selaya, N. G., Sillett, S. C., Sterck, F., Takagi, K., Tange, T., Tanouchi, H., Tissue, D., Umehara, T., Utsugi, H., Vadeboncoeur, M. A., Valladares, F., Vanninen, P., Wang, J. R., Wenk, E., Williams, R., de Aquino Ximenes, F., Yamaba, A., Yamada, T., Yamakura, T., Yanai, R. D., and York, R. A.: BAAD: a Biomass And Allometry Database for woody plants, Ecology, 96, 1445–1445, https://doi.org/10.1890/14-1889.1, 2015.

Forkel, M., Schmidt, L., Zotta, R.-M., Dorigo, W., and Yebra, M.: Estimating leaf moisture content at global scale from passive microwave satellite observations of vegetation optical depth, Hydrol. Earth Syst. Sci. Discuss., 1–43, https://doi.org/10.5194/hess-2022-121, 2022.

Fuster, B., Sánchez-Zapero, J., Camacho, F., García-Santos, V., Verger, A., Lacaze, R., Weiss, M., Baret, F., and Smets, B.: Quality Assessment of PROBA-V LAI, fAPAR and fCOVER Collection 300 m Products of Copernicus Global Land Service, Remote Sens., 12, 1017, https://doi.org/10.3390/rs12061017, 2020.

Kattge, J., Díaz, S., Lavorel, S., Prentice, I. C., Leadley, P., Bönisch, G., Garnier, E., Westoby, M., Reich, P. B., Wright, I. J., Cornelissen, J. H. C., Violle, C., Harrison, S. P., van Bodegom, P. M., Reichstein, M., Enquist, B. J., Soudzilovskaia, N. A., Ackerly, D. D., Anand, M., Atkin, O., Bahn, M., Baker, T. R., Baldocchi, D., Bekker, R., Blanco, C. C., Blonder, B., Bond, W. J., Bradstock, R., Bunker, D. E., Casanoves, F., Cavender-Bares, J., Chambers, J. Q., Chapin Iii, F. S., Chave, J., Coomes, D., Cornwell, W. K., Craine, J. M., Dobrin, B. H., Duarte, L., Durka, W., Elser, J., Esser, G., Estiarte, M., Fagan, W. F., Fang, J., Fernández-Méndez, F., Fidelis, A., Finegan, B., Flores, O., Ford, H., Frank, D., Freschet, G. T., Fyllas, N. M., Gallagher, R. V., Green, W. A., Gutierrez, A. G., Hickler, T., Higgins, S. I., Hodgson, J. G., Jalili, A., Jansen, S., Joly, C. A., Kerkhoff, A. J., Kirkup, D., Kitajima, K., Kleyer, M., Klotz, S., Knops, J. M. H., Kramer, K., Kühn, I., Kurokawa, H., Laughlin, D., Lee, T. D., Leishman, M., Lens, F., Lenz, T., Lewis, S. L., Lloyd, J., Llusià, J., Louault, F., Ma, S., Mahecha, M. D., Manning, P., Massad, T., Medlyn, B. E., Messier, J., Moles, A. T., Müller, S. C., Nadrowski, K., Naeem, S., Niinemets, Ü., Nöllert, S., Nüske, A., Ogaya, R., Oleksyn, J., Onipchenko, V. G., Onoda, Y., Ordoñez, J., Overbeck, G., et al.: TRY – a global database of plant traits, Glob. Change Biol., 17, 2905–2935, https://doi.org/10.1111/j.1365-2486.2011.02451.x, 2011.

de Laat, A., Vazquez-Navarro, M., Theys, N., and Stammes, P.: Analysis of properties of the 19 February 2018 volcanic eruption of Mount Sinabung in S5P/TROPOMI and Himawari-8 satellite data, Nat. Hazards Earth Syst. Sci., 20, 1203–1217, https://doi.org/10.5194/nhess-20-1203-2020, 2020.

van Leeuwen, T. T., van der Werf, G. R., Hoffmann, A. A., Detmers, R. G., Rücker, G., French, N. H. F., Archibald, S., Carvalho Jr., J. A., Cook, G. D., de Groot, W. J., Hély, C., Kasischke, E. S., Kloster, S., McCarty, J. L., Pettinari, M. L., Savadogo, P., Alvarado, E. C., Boschetti, L., Manuri, S., Meyer, C. P., Siegert, F., Trollope, L. A., and Trollope, W. S. W.: Biomass

burning fuel consumption rates: a field measurement database, Biogeosciences, 11, 7305–7329, https://doi.org/10.5194/bg-11-7305-2014, 2014.

Moesinger, L., Dorigo, W., Jeu, R. de, Schalie, R. van der, Scanlon, T., Teubner, I., and Forkel, M.: The global long-term microwave Vegetation Optical Depth Climate Archive (VODCA), Earth Syst. Sci. Data, 12, 177–196, https://doi.org/10.5194/essd-12-177-2020, 2020.

Pettinari, M. L. and Chuvieco, E.: Generation of a global fuel data set using the Fuel Characteristic Classification System, Biogeosciences, 13, 2061–2076, https://doi.org/10.5194/bg-13-2061-2016, 2016.

Potapov, P., Li, X., Hernandez-Serna, A., Tyukavina, A., Hansen, M. C., Kommareddy, A., Pickens, A., Turubanova, S., Tang, H., Silva, C. E., Armston, J., Dubayah, R., Blair, J. B., and Hofton, M.: Mapping global forest canopy height through integration of GEDI and Landsat data, Remote Sens. Environ., 253, 112165, https://doi.org/10.1016/j.rse.2020.112165, 2021a.

Potapov, P., Li, X., Hernandez-Serna, A., Tyukavina, A., Hansen, M. C., Kommareddy, A., Pickens, A., Turubanova, S., Tang, H., Silva, C. E., Armston, J., Dubayah, R., Blair, J. B., and Hofton, M.: Mapping global forest canopy height through integration of GEDI and Landsat data, Remote Sens. Environ., 253, 112165, https://doi.org/10.1016/j.rse.2020.112165, 2021b.

Prichard, S. J., Kennedy, M. C., Andreu, A. G., Eagle, P. C., French, N. H., and Billmire, M.: Next-Generation Biomass Mapping for Regional Emissions and Carbon Inventories: Incorporating Uncertainty in Wildland Fuel Characterization, J. Geophys. Res. Biogeosciences, 124, 3699–3716, https://doi.org/10.1029/2019JG005083, 2019.

Rémy, S., Veira, A., Paugam, R., Sofiev, M., Kaiser, J. W., Marenco, F., Burton, S. P., Benedetti, A., Engelen, R. J., Ferrare, R., and others: Two global data sets of daily fire emission injection heights since 2003, Atmospheric Chem. Phys., 17, 2921–2942, 2017.

Roteta, E., Bastarrika, A., Franquesa, M., and Chuvieco, E.: Landsat and Sentinel-2 Based Burned Area Mapping Tools in Google Earth Engine, Remote Sens., 13, 816, https://doi.org/10.3390/rs13040816, 2021.

Santoro, M., Cartus, O., Carvalhais, N., Rozendaal, D. M. A., Avitabile, V., Araza, A., de Bruin, S., Herold, M., Quegan, S., Rodríguez-Veiga, P., Balzter, H., Carreiras, J., Schepaschenko, D., Korets, M., Shimada, M., Itoh, T., Moreno Martínez, Á., Cavlovic, J., Cazzolla Gatti, R., da Conceição Bispo, P., Dewnath, N., Labrière, N., Liang, J., Lindsell, J., Mitchard, E. T. A., Morel, A., Pacheco Pascagaza, A. M., Ryan, C. M., Slik, F., Vaglio Laurin, G., Verbeeck, H., Wijaya, A., and Willcock, S.: The global forest above-ground biomass pool for 2010 estimated from high-resolution satellite observations, Earth Syst. Sci. Data, 13, 3927–3950, https://doi.org/10.5194/essd-13-3927-2021, 2021.

Shvetsov, E. G., Kukavskaya, E. A., Buryak, L. V., and Barrett, K.: Assessment of post-fire vegetation recovery in Southern Siberia using remote sensing observations, Environ. Res. Lett., 14, 055001, https://doi.org/10.1088/1748-9326/ab083d, 2019.

Val Martin, M., Logan, J. A., Kahn, R. A., Leung, F.-Y., Nelson, D. L., and Diner, D. J.: Smoke injection heights from fires in North America: analysis of 5 years of satellite observations, Atmospheric Chem. Phys., 10, 1491–1510, https://doi.org/10.5194/acp-10-1491-2010, 2010.

Veira, A., Kloster, S., Wilkenskjeld, S., and Remy, S.: Fire emission heights in the climate system – Part 1: Global plume height patterns simulated by ECHAM6-HAM2, Atmospheric Chem. Phys., 15, 7155–7171, https://doi.org/10.5194/acp-15-7155-2015, 2015.

Walker, X. J., Rogers, B. M., Veraverbeke, S., Johnstone, J. F., Baltzer, J. L., Barrett, K., Bourgeau-Chavez, L., Day, N. J., de Groot, W. J., Dieleman, C. M., Goetz, S., Hoy, E., Jenkins, L. K., Kane, E. S., Parisien, M.-A., Potter, S., Schuur, E. a. G., Turetsky, M., Whitman, E., and Mack, M. C.: Fuel availability not fire weather controls boreal wildfire severity and carbon emissions, Nat. Clim. Change, 10, 1130–1136, https://doi.org/10.1038/s41558-020-00920-8, 2020.

Wang, L., Quan, X., He, B., Yebra, M., Xing, M., and Liu, X.: Assessment of the Dual Polarimetric Sentinel-1A Data for Forest Fuel Moisture Content Estimation, Remote Sens., 11, 1568, https://doi.org/10.3390/rs11131568, 2019.

van der Werf, G. R., Randerson, J. T., Giglio, L., Van Leeuwen, T. T., Chen, Y., Rogers, B. M., Mu, M., Van Marle, M. J., Morton, D. C., Collatz, G. J., and others: Global fire emissions estimates during 1997-2016, Earth Syst. Sci. Data, 9, 697–720, 2017.

Yebra, M., Scortechini, G., Badi, A., Beget, M. E., Boer, M. M., Bradstock, R., Chuvieco, E., Danson, F. M., Dennison, P., Dios, V. R. de, Bella, C. M. D., Forsyth, G., Frost, P., Garcia, M., Hamdi, A., He, B., Jolly, M., Kraaij, T., Martín, M. P., Mouillot, F., Newnham, G., Nolan, R. H., Pellizzaro, G., Qi, Y., Quan, X., Riaño, D., Roberts, D., Sow, M., and Ustin, S.: Globe-LFMC, a global plant water status database for vegetation ecophysiology and wildfire applications, Sci. Data, 6, 1–8, https://doi.org/10.1038/s41597-019-0164-9, 2019.